International Communications in Heat and Mass Transfer 49 (2013) 10–16

Contents lists available at ScienceDirect

International Communications in Heat and Mass Transfer

journal homepage: www.elsevier.com/locate/ichmt

Turbulent free convection in a porous square cavity using the thermal equilibirum model☆

Paulo H.S. Carvalho, Marcelo J.S. de Lemos *

Departamento de Energia — IEME, Instituto Tecnológico de Aeronáutica — ITA, 12228-900 São José dos Campos — SP, Brazil

ARTICLE INFO

Available online 29 October 2013

Keywords:
Turbulence modeling
Porous media
Heat transfer
Natural convection

ABSTRACT

This work investigates the influence of porosity and thermal conductivity ratio on the Nusselt number of a cavity filed with a fluid saturated porous substrate. The flow regime considered intra-pore turbulence and a macroscopic k-ε model was applied. Heat transfer across the cavity assumed the hypothesis of thermal equilibrium between the solid and the fluid phases. Transport equations were discretized using the control-volume method and the system of algebraic equations was relaxed via the SIMPLE algorithm. Results showed that when using the one energy equation model under the turbulent regime, simulated with a High Reynolds turbulence model, the cavity Nusselt number is reduced for higher values of the ratio k_s/k_f as well as when the material porosity is increased. In both cases, conduction thorough the solid material becomes of a greater importance when compared with the overall transport that includes both convection and conduction mechanisms across the medium.

1. Introduction

Thermal convection in porous media and the parameters that affect heat transfer across a heterogeneous medium have been studied extensively in recent years. There are several applications in industry for this type of technology. Examples are studies on grain storage, optimization of solar collectors design, safety of nuclear reactors and design of porous burners for industrial furnaces, to mention a few. Traditionally, modeling of macroscopic transport for incompressible flows in porous media has been based on the volume-average methodology [1–4]. Additionally, if the flow fluctuates in time, the literature presents a number of time- and volume-averaging techniques that follow distinct sequences when applying both averaging operators [5–11]. Recently, a concept named *double decomposition* [12] showed that the sets of macroscopic mass transport equations are equivalent, regardless of the order of application of the averaging operators.

When buoyancy forces are of concern, natural convection occurs in enclosures as a result of gradients in densities which, in turn, are due to variations in temperature or mass concentration within the medium.

For clear cavities, the first turbulence model introduced for calculating buoyant flows was proposed by Markatos and Pericleous [13]. They performed steady 2-D simulations for Ra up to 10^{16} and presented a complete set of results. Ozoe et al. [14], in the light of the same model adopted by [13], applied it to 2D calculations up to $Ra = 10^{11}$. Henkes et al. [15] compared two different turbulence models for 2D calculations, namely the standard High Reynolds k-ε closure as well as the Low–Reynolds number form of the model. Further, Fusegi et al. [16] presented 3D calculations for laminar flow for Ra up to 10^{10} in a cube. The results revealed that the behaviors of the flow and comparisons were made with 2D simulations. The differences were reported considering heat transfer correlation between Nu and Ra for 2D and 3D cases. Later, Barakos et al. [17] also studied the problem of natural convection flow in a clean square cavity. The k-ε model has been used for modeling turbulence with and without wall functions.

For cavities fitted with a porous material, the problem of free convection in enclosures with distinct temperatures applied on each side of the cavity has been shown to represent a number of engineering systems of practical relevance. The monographs of Nield and Bejan [18] and Ingham and Pop [19] fully document natural convection in porous media. In addition, several articles published in the literature made important contributions to the understanding of this problem [20–26]. Baytas and Pop [27] considered a numerical study of steady free convection flow in rectangular and oblique cavities, filled with homogeneous porous media using a nonlinear axis transformation. The Darcy momentum and energy equations were numerically solved using the (ADI) method.

In the work of Braga and de Lemos (2004) [28], an approximate critical Rayleigh was proposed comparing the behavior of Laminar and High Reynolds turbulence model solutions. The geometry there investigated was a square cavity totally filled with a porous material, which was heated from the left and cooled from the opposing side. Also worth to mention is that the work in [28] was based on the local thermal equilibrium (LTE) hypothesis, which considers one unique temperature for both the fluid and the solid porous material. Other cases not involving gravity driven motion [29] have also been analyzed with the laminar version of the LTE model detailed in [12]. Further, in

☆ Communicated by Dr. W.J. Minkowycz.

* Corresponding author.
E-mail address: delemos@ita.br (M.J.S. de Lemos).

0735-1933/$ – see front matter © 2013 Elsevier Ltd. All rights reserved.
http://dx.doi.org/10.1016/j.icheatmasstransfer.2013.10.003

Nomenclature

Latin characters

c_F	Forchheimer coefficient
$c's$	Non-dimensional turbulence model constants
c_p	Specific heat
$\mathbf{D}$	Deformation rate tensor, $\mathbf{D}=[\nabla\mathbf{u}+(\nabla\mathbf{u})^T]/2$
Da	Darcy number, $Da=\frac{K}{H^2}$
D	Particle diameter, D
$\mathbf{g}$	Gravity acceleration vector
G^i	Generation rate of $\langle k\rangle^i$ due to the action of the porous matrix
$G^i_{f\beta}$	Generation rate of $\langle k\rangle^i$ due to buoyant effects
h	Heat transfer coefficient
H	Cavity height
$\mathbf{I}$	Unit tensor
K	Permeability, $K=\frac{D^2\phi^3}{144(1-\phi)^2}$
k	Turbulent kinetic energy per unit mass, $k=\overline{\mathbf{u}'\cdot\mathbf{u}'}/2$
k_f	Fluid thermal conductivity
k_s	Solid thermal conductivity
$\mathbf{K}_{disp}$	Conductivity tensor due to thermal dispersion
$\mathbf{K}_{disp,t}$	Conductivity tensor due to turbulent thermal dispersion
$\mathbf{K}_t$	Conductivity tensor due to turbulent heat flux
$\mathbf{K}_{tor}$	Conductivity tensor due to tortuosity
L	Cavity width
Nu	Nusselt number, $Nu={}^{hL}/_{k_{eff}}$
P^i	Production rate of $\langle k\rangle^i$ due to gradients of $\overline{\mathbf{u}}_D$
Pr	Prandtl number
Ra_f	Macroscopic Fluid Rayleigh number, $Ra_f=\frac{g\beta_\phi H^3\Delta T}{\nu_f\alpha_{eff}}$
Ra_m	Darcy–Rayleigh number, $Ra_m=Ra_f\cdot Da=\frac{g\beta_\phi H\Delta TK}{\nu_f\alpha_{eff}}$
Ra_{cr}	Critical Rayleigh number
Re_D	Reynolds number based on the particle diameter, $\mathrm{Re}_D=\frac{\rho\lvert\overline{\mathbf{u}}_D\rvert D}{\mu_f}$
T	Temperature
$\mathbf{u}$	Microscopic velocity
$\mathbf{u}_D$	Darcy or superficial velocity (volume average of $\mathbf{u}$)

Greek characters

α	Thermal diffusivity
β	Thermal expansion coefficient
ΔV	Representative elementary volume
ΔV_f	Fluid volume inside ΔV
ε	$\varepsilon=\mu\nabla\mathbf{u}':(\nabla\mathbf{u}')^T/\rho$, Dissipation rate of k
μ	Dynamic viscosity
μ_t	Microscopic turbulent viscosity
μ_{t_ϕ}	Macroscopic turbulent viscosity
ν	Kinematic viscosity
ρ	Density
$\sigma's$	Non-dimensional constants
ϕ	$\phi={}^{\Delta V_f}/_{\Delta V}$, Porosity

Special characters

φ	General variable
$\overline{\varphi}$	Time average
φ'	Time fluctuation
$\langle\varphi\rangle^i$	Intrinsic average
$\langle\varphi\rangle^v$	Volume average
${}^i\varphi$	Spatial deviation
$\lvert\varphi\rvert$	Absolute value (Abs)
$\boldsymbol{\varphi}$	General vector variable
φ_{eff}	Effective value of φ, $\varphi_{eff}=\phi\varphi_f+(1-\phi)\varphi_s$
$\varphi_{s,f}$	solid/fluid
$\varphi_{H,C}$	Hot/cold
φ_ϕ	Macroscopic value
$()^T$	Transpose

[28] it was also shown that low Darcy numbers impact in higher average Nusselt numbers at the hot wall. However, in reference [28] simulations were limited to a single solid-to-fluid thermal conductivity ratio, $k_s/k_f=1$, and a single porosity value, $\phi=0.8$.

Motivated by the foregoing work, the contribution of this work is to extend the findings in [28] varying now the ratio k_s/k_f and the porosity ϕ. The turbulence model here adopted is the macroscopic k-ε with wall function in addition to the Low Reynolds number version of the model. The findings herein broaden the simulations presented earlier in [28] since a greater number of heterogonous systems are now investigated, leading to the analysis and optimization of a wider range of practical engineering systems.

2. The problem under consideration

The problem considered is showed schematically in Fig. 1a and refers to a square cavity with sides $L=H=1$ m completely filled with a porous medium. The cavity is isothermally heated from the left, T_H, and cooled from the opposing side, T_C. The other two walls are thermally insulated. These boundary conditions are widely applied when solving buoyancy-driven cavity flows. The porous medium is considered to be rigid and saturated by an incompressible fluid. The modified Rayleigh number, Ra_m, is a dimensionless parameter used in porous media

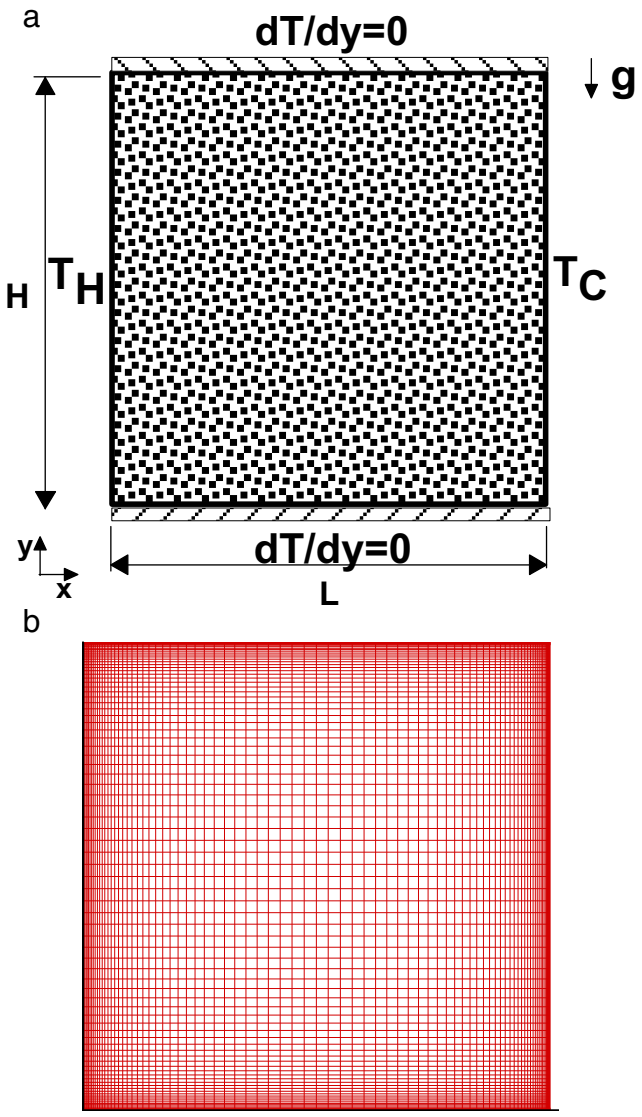

Fig. 1. a) Geometry under consideration; b) 80×80 stretched grid.

analysis and it is defined as $Ra_m = Ra_f Da$, where $Da = K/H^2$, $\alpha_{eff} = {k_{eff}}/{(\rho c_p)_f}$. D is the particle diameter used to calculate the permeability, K, and is here given by $D = \sqrt{\frac{144K(1-\phi)^2}{\phi^3}}$.

3. Governing equations

For turbulent buoyant flows, macroscopic governing equations are obtained by taking both volumetric and time averaging of the entire equation set. The final forms of the equations considered here are given in detail in [12] and for this reason their derivation need not be repeated. They read:

Continuity:

$$\nabla \cdot \overline{\mathbf{u}}_D = 0 \tag{1}$$

Momentum:

$$\rho\left[\frac{\partial \overline{\mathbf{u}}_D}{\partial t} + \nabla\cdot\left(\frac{\overline{\mathbf{u}}_D\overline{\mathbf{u}}_D}{\phi}\right)\right] = -\nabla\left(\phi\langle\overline{p}\rangle^i\right) + \mu\nabla^2\overline{\mathbf{u}}_D + \nabla\cdot\left(-\rho\phi\left\langle\overline{\mathbf{u}'\mathbf{u}'}\right\rangle^i\right) - \rho\beta_\phi\mathbf{g}\phi\left(\langle\overline{T}\rangle^i - T_{ref}\right) - \left[\frac{\mu\varphi}{K}\overline{\mathbf{u}}_D + \frac{c_F\phi\rho|\overline{\mathbf{u}}_D|\overline{\mathbf{u}}_D}{\sqrt{K}}\right] \tag{2}$$

Turbulent kinetic energy:

$$\rho\left[\frac{\partial}{\partial t}\left(\phi\langle k\rangle^i\right) + \nabla\cdot\left(\overline{\mathbf{u}}_D\langle k\rangle^i\right)\right] = \nabla\cdot\left[\left(\mu + \frac{\mu_{t_\phi}}{\sigma_k}\right)\nabla\left(\phi\langle k\rangle^i\right)\right] + P^i + G^i + G^i_\beta - \rho\phi\langle\varepsilon\rangle^i \tag{3}$$

Dissipation rate of turbulence kinetic energy:

$$\rho\left[\frac{\partial}{\partial t}\left(\phi\langle\varepsilon\rangle^i\right) + \nabla\cdot\left(\overline{\mathbf{u}}_D\langle\varepsilon\rangle^i\right)\right] = \nabla\cdot\left[\left(\mu + \frac{\mu_{t_\phi}}{\sigma_\varepsilon}\right)\nabla\left(\phi\langle\varepsilon\rangle^i\right)\right] + c_1P^i\frac{\langle\varepsilon\rangle^i}{\langle k\rangle^i} + c_2\frac{\langle\varepsilon\rangle^i}{\langle k\rangle^i}G^i + c_1c_3G^i_\beta\frac{\langle\varepsilon\rangle^i}{\langle k\rangle^i} - c_2f_2\rho\phi\frac{\langle\varepsilon\rangle^{i2}}{\langle k\rangle^i} \tag{4}$$

where the Dupuit–Forchheimer relationship, $\overline{\mathbf{u}}_D = \phi\langle\overline{\mathbf{u}}\rangle^i$, has been used and $\langle\overline{\mathbf{u}}\rangle^i$ identifies the intrinsic (liquid) average of the local velocity vector $\overline{\mathbf{u}}$, $\langle k\rangle^i$ is the intrinsic average for k, $\langle\varepsilon\rangle^i$ is the intrinsic dissipation rate of k, K is the medium permeability, $G^i = c_k\rho\phi\,\langle k\rangle^i|\overline{\mathbf{u}}_D|/\sqrt{K}$ is the generation rate of $\langle k\rangle^i$ due to the action of the porous matrix, $G^i_\beta = \phi\frac{\mu_{t_\phi}}{\sigma_t}\beta^k_\phi\mathbf{g}\cdot\nabla\langle\overline{T}\rangle^i$ is the generation rate of $\langle k\rangle^i$ due to buoyant effects, $\beta_\phi = \frac{\langle\rho\beta(T-T_{ref})\rangle^v}{\rho\phi\left(\langle T\rangle^i - T_{ref}\right)}$ is the macroscopic thermal expansion coefficient and $\beta^k_\phi = \frac{\langle\beta\mathbf{u}'T'\rangle^v}{\phi\left\langle\mathbf{u}'T'_f\right\rangle^i}$ is the macroscopic thermal coefficient appearing in the G^i_β term. Here, for simplicity, we assume $\beta^k_\phi = \beta_\phi = \beta$ (see [12] for details). Further, $P^i = -\rho\left\langle\overline{\mathbf{u}'\mathbf{u}'}\right\rangle^i : \nabla\overline{\mathbf{u}}_D$ is the production rate of $\langle k\rangle^i$ due to gradients of $\overline{\mathbf{u}}_D$, the c's are constants and f_2 is a damping function to be commented upon later. The term $-\rho\phi\left\langle\overline{\mathbf{u}'\mathbf{u}'}\right\rangle^i$ is known as the macroscopic Reynolds stress tensor (MRST) and is given by:

$$-\rho\phi\left\langle\overline{\mathbf{u}'\mathbf{u}'}\right\rangle^i = \mu_{t_\phi}2\langle\overline{\mathbf{D}}\rangle^{\mathbf{v}} - \frac{2}{3}\phi\rho\langle k\rangle^i\mathbf{I} \tag{5}$$

where

$$\langle\overline{\mathbf{D}}\rangle^v = \frac{1}{2}\left[\nabla\left(\phi\langle\overline{\mathbf{u}}\rangle^i\right) + \left[\nabla\left(\phi\langle\overline{\mathbf{u}}\rangle^i\right)\right]^T\right] \tag{6}$$

is the macroscopic deformation rate tensor. The macroscopic turbulent viscosity μ_{t_ϕ} is modeled as,

$$\mu_{t_\phi} = \rho\, c_\mu f_\mu \frac{\langle k\rangle^{i2}}{\langle\varepsilon\rangle^i} \tag{7}$$

where c_μ is a constant and f_μ is another damping function to be presented below.

In a similar way, applying both time and volumetric average to the microscopic energy equation and invoking the Local Thermal Equilibrium Hypothesis, which considers as mentioned $\langle\overline{T_f}\rangle^i = \langle\overline{T_s}\rangle^i = \langle\overline{T}\rangle^i$, a modeled form for the macroscopic energy equation reads (see [12]),

$$\left\{\left(\rho c_p\right)_f\phi + \left(\rho c_p\right)_s(1-\phi)\right\}\frac{\partial\langle\overline{T}\rangle^i}{\partial t} + \left(\rho c_p\right)_f\nabla\cdot\left(\overline{\mathbf{u}}_D\langle\overline{T}\rangle^i\right) = \nabla\cdot\left\{\mathbf{K}_{eff}\cdot\nabla\langle\overline{T}\rangle^i\right\} \tag{8}$$

where, K_{eff}, given by:

$$\mathbf{K}_{eff} = \left[\phi k_f + (1-\phi)k_s\right]\mathbf{I} + \mathbf{K}_{tor} + \mathbf{K}_t + \mathbf{K}_{disp} + \mathbf{K}_{disp,t} \tag{9}$$

is the effective conductivity tensor. In order to be able to apply Eq. (8), it is necessary to determine the conductivity tensors in Eq. (9), i.e. $\mathbf{K}_{tor}$, $\mathbf{K}_t$, $\mathbf{K}_{disp}$ and $\mathbf{K}_{disp,t}$. The turbulent heat flux and turbulent thermal dispersion terms, $\mathbf{K}_t$ and $\mathbf{K}_{disp,t}$ are modeled such that,

$$-\phi\left(\rho c_p\right)_f\left\langle\overline{\mathbf{u}'T'}\right\rangle^i = \phi\left(\rho c_p\right)_f\frac{\nu_{t_\phi}}{Pr_t}\nabla\langle\overline{T}\rangle^i = \left(\mathbf{K}_t + \mathbf{K}_{disp,t}\right)\cdot\nabla\langle\overline{T}\rangle^i \tag{10}$$

Table 1
Damping functions and constants for High and Low Reynolds turbulence models.

High Reynolds model proposed by Launder and Spalding [30]		Low Reynolds model proposed by Abe et al. [31]
f_μ	1.0	$\left\{1-\exp\left[-\frac{(\nu\varepsilon)^{0.25}y}{14\nu}\right]\right\}^2\left\{1+\frac{5}{(k^2/\nu\varepsilon)^{0.75}}\exp\left[-\left(\frac{(k^2/\nu\varepsilon)}{200}\right)^2\right]\right\}$
f_2	1.0	$\left\{1-\exp\left[-\frac{(\nu\varepsilon)^{0.25}y}{3.1\nu}\right]\right\}^2\left\{1-0.3\exp\left[-\left(\frac{(k^2/\nu\varepsilon)}{6.5}\right)^2\right]\right\}$
σ_k	1.0	1.4
σ_ε	1.33	1.3
c_1	1.44	1.5
c_2	1.92	1.9

Table 2
Comparison of laminar results for average Nusselt at hot wall, Nu_w, with Ra_m varying from 10 until 10^4, $Da = 10^{-7}$, $\phi = 0.8$ and $k_s/k_f = 1$.

	Ra_m			
	10	10^2	10^3	10^4
Walker and Homsy [20]	–	3.097	12.96	51.0
Bejan [21]	–	4.2	15.8	50.8
Beckermann et al. [23]	–	3.113	–	48.9
Gross et al. [24]	–	3.141	13.448	42.583
Manole and Lage [25]	–	3.118	13.637	48.117
Moya et al. [26]	1.065	2.801	–	–
Baytas and Pop [27]	1.079	3.16	14.06	48.33
Braga and de Lemos [28]	1.090	3.086	12.931	38.971
Present results	1.087	3.093	13.041	39.288

Table 3
Effect of simulation model on average Nusselt at hot wall, Nu_w, with $Da = 10^{-7}$, $\phi = 0.8$, and $k_s/k_f = 1$.

	Ra_m			
	10^3	10^4	10^5	10^6
Braga and de Lemos [28] (HR)	13.032	40.614	101.647	237.546
High Re turbulence model	13.271	41.792	101.503	234.930
Low Re turbulence model, $y^+_W = 0.767$	13.132	40.602	96.918	–
Laminar model	13.041	39.288	88.238	172.491

where the symbol ν_{t_ϕ} expresses the macroscopic kinematic eddy viscosity such that $\mu_{t_\phi} = \rho_f \nu_{t_\phi}$ and Pr_t is a constant known as turbulent Prandtl number, which is often represented in the literature by σ_t. A further simplification is that, under the conditions here studied, K_{tor} and K_{disp} are negligible when compared to $\mathbf{K}_t$ K_t and K_{disp} [28].

3.1. Wall treatment and boundary conditions

In this work, two forms of the k-ε model are employed, namely the High Reynolds (Launder and Spalding [30]) and Low Reynolds number (Abe et al. [31]) turbulence models. The constants and formulae used as damping functions are shown in Table 1. Boundary conditions are given by:

On the solid walls (Low Reynolds turbulence model):

$$\overline{u} = 0, \quad k = 0, \quad \varepsilon = \nu \frac{\partial^2 k}{\partial y^2} \tag{11}$$

On the solid walls (High Reynolds turbulence model):

$$\frac{\overline{u}}{u_\tau} = \frac{1}{\kappa} \ln\left(y^+ E\right), \quad k = \frac{u_\tau^2}{c_\mu^{1/2}}, \quad \varepsilon = \frac{c_\mu^{3/4} k_w^{3/2}}{\kappa y_w}, \quad q_w = \frac{\left(\rho c_p\right)_f c_\mu^{1/4} k_w^{1/2} \left(\overline{T} - T_w\right)}{\left(\frac{Pr_t}{\kappa} \ln\left(y_w^+\right) + c_Q(Pr)\right)} \tag{12}$$

with, $u_\tau = \left(\frac{\tau_w}{\rho}\right)^{1/2}$, $y_w^+ = \frac{y_w u_\tau}{\nu}$, $c_Q = 12.5 Pr^{2/3} + 2.12 \ln(Pr) - 5.3$ for $Pr > 0.5$ where, Pr and Pr_t are, as mentioned, the Prandtl and turbulent Prandtl numbers, respectively, q_w is the wall heat flux, u_τ is the wall-friction velocity, y_w is the non-dimensional coordinate normal to wall, K is the von Kármán constant, and E is a constant that depends on the roughness of the wall.

4. Numerical method and solution procedure

The numerical method employed for discretizing the governing equations is the control-volume approach. Hybrid schemes, upwind

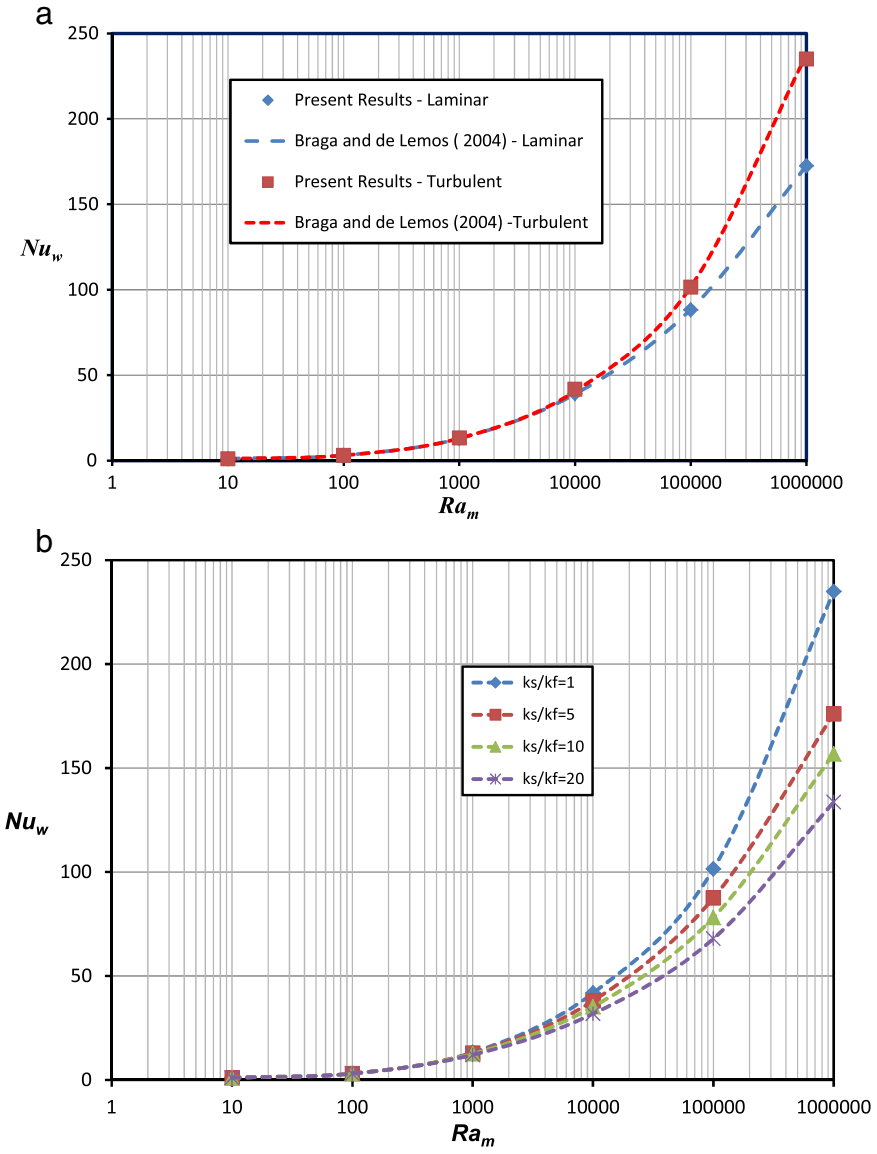

Fig. 2. Average Nusselt at hot wall Nu_w for $\phi = 0.8$, $D = 1.06 \times 10^{-3}$m, $Da = 10^{-7}$ and 80×80 stretched grid: a) Laminar and High Reynolds turbulence models, $k_s/k_f = 1$, b) High Reynolds turbulence model, varying k_s/k_f.

differencing scheme (UDS) and central differencing scheme (CDS), are used for interpolating the convection fluxes. The well-established SIMPLE algorithm [32] is applied for handling the pressure–velocity coupling. Algebraic equation sets for each variable were solved by the SIP procedure of [33]. In addition, the concentration of nodal points close to the walls aims at capturing the boundary layers close to the solid surfaces.

5. Results and discussion

To guarantee a grid independent solution, runs were performed using stretched grids with 60×60, 80×80, 100×100 control volumes and $Ra_m = 10^5$. In these three cases, the average Nusselt number at the hot wall showed that the grid 80×80 is refined enough to capture the boundary layers at vertical surfaces, since the difference in the results was less than 2% when compared with similar simulations obtained with a finer grid. For example, for $Ra_m = 10^5$ and for a grid with 80×80 nodes (Fig. 1b), the average Nusselt at hot wall was calculated as 101.503, whereas for a mesh of size 100×100, the computed value was 103.38. As such, a grid of size 80×80 was chosen for all simulations herein.

Further, the local Nusselt number on the hot wall for the square cavity at $x = 0$ is defined as,

$$Nu = hL/k_{eff} \therefore Nu = \left(\frac{q_W}{k_{eff}}\right)_{x=0} \frac{L}{T_H - T_C} \tag{13}$$

and the average Nusselt number is given by,

$$Nu_w = \frac{1}{H}\int_0^H Nu\, dy. \tag{14}$$

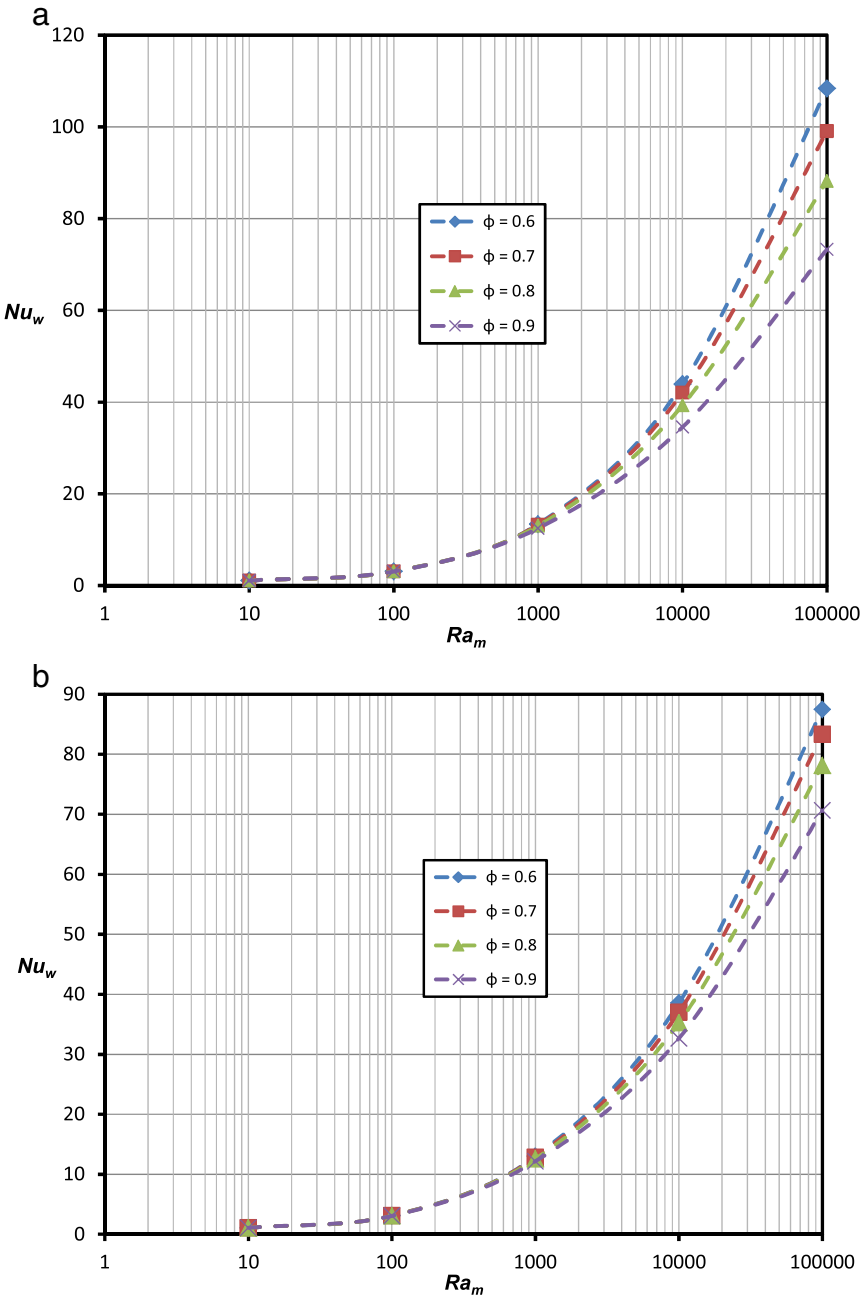

Fig. 3. Effects of porosity on average Nusselt at hot wall, Nu_w, using the HR turbulence model, $D = 1.06 \times 10^{-3}$m: a) $k_s/k_f = 1$, b) $k_s/k_f = 10$.

6. Laminar model solution

In order to calibrate the solution, runs were performed using the stretched grid shown in Fig. 1b. Results are presented shown in Table 2 and compared with the literature for $\varphi = 0.8$ and $Da = 10^{-7}$. In all results, the Prandtl Number, thermal conductivity ratio between solid and fluid phases, fluid density and specific heat considered were taken as unity. As one can see in Table 2, the present results agree well with those reported in the literature.

7. Turbulent model solution

7.1. High Reynolds turbulence model

As Braga and de Lemos [28] pointed out, it is important to emphasize that the main objective of this work is not to simulate the transition mechanism from laminar regime to fully turbulent flow, but rather identify the ranges of validity of each model. Here, a 80×80 stretched grid has been used and the results are compared with those in [28] in Table 3 for Ra_m ranging from 10 to 10^6. Table 3 also presents results using the Laminar model. As can be seen in Table 3 and Fig. 2a, the critical Rayleigh number, Ra_{cr}, is assumed to be the value when the two solutions deviate from each other. Here, the computed Ra_{cr} also agrees with that proposed in Braga and de Lemos [28] as $Ra_{cr} = 10^4$ for $k_s/k_f = 1$.

7.2. Low Reynolds turbulence model

It is known that Low Reynolds turbulence models make use of damping functions and require that the first grid node close to the wall corresponds to a non-dimensional wall distance of about $y_w^+ \approx 1$. Going back to Table 3, one can note that for Ra_m up to 10^4, calculated Nusselt are similar, regardless of the model used, namely HR, LR or Laminar models. After such value, here considered as a critical value, Ra_{cr}, the role of the model used becomes important when obtaining Nu_w.

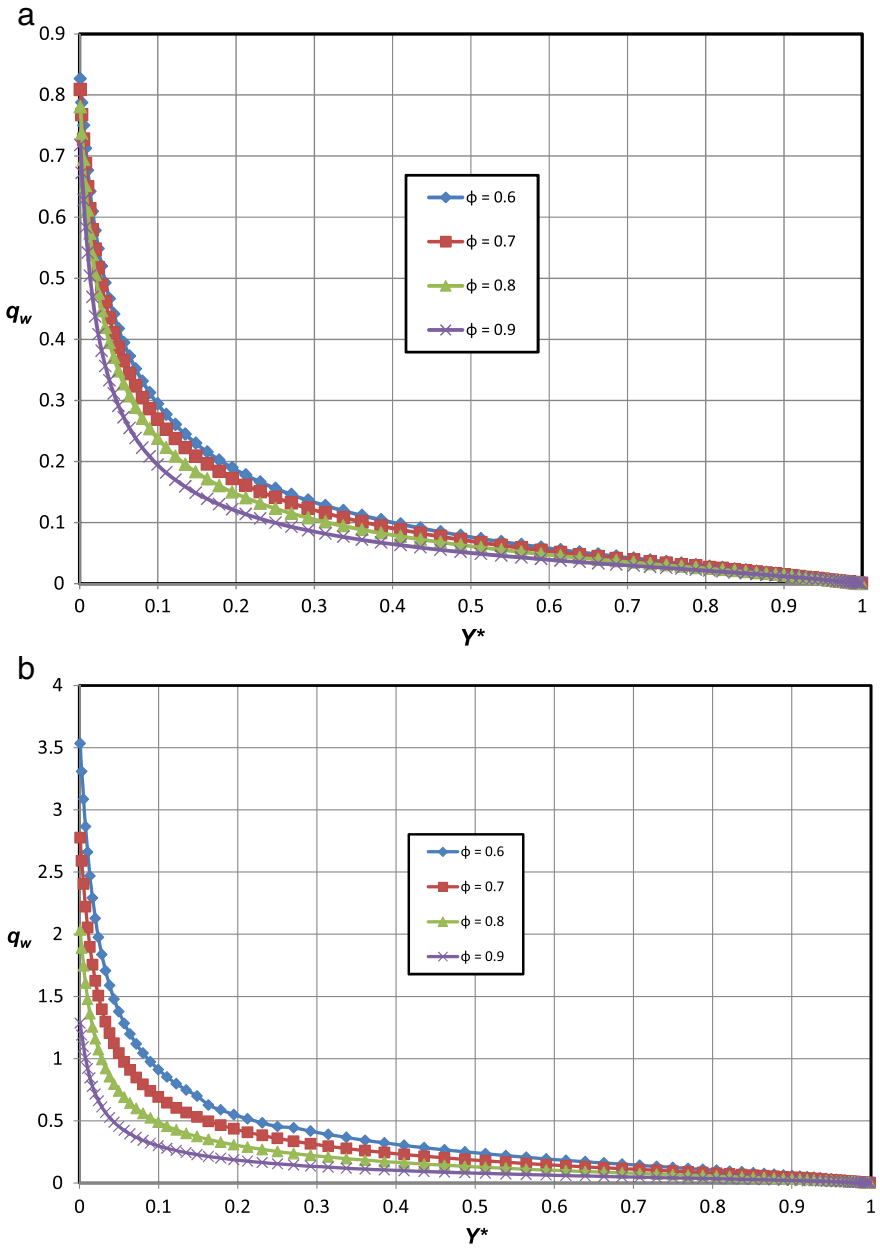

Fig. 4. Overall heat flux along hot wall using the HR turbulence model, $D = 1.06 \times 10^{-3}$m, $Ra_m = 10^5$: a) $k_s/k_f = 1$, b) $k_s/k_f = 10$.

8. Effect of thermal conductivity ratio k_s/k_f

The ratio between the solid and fluid thermal conductivity plays an important role in the study of energy transport across saturated porous media. To the best of the authors' knowledge, in all published materials the ratio k_s/k_f has been set to unit. However, for real engineering problems, such ratio may attain higher values and, for that, a study for obtaining Nu_w with a varying ratio k_s/k_f is here included.

Fig. 2b shows values for Nu_w when k_s/k_f is varied from 1 to 20 for a range for Ra_m covering 10 to 10^6 and using the High Reynolds turbulence model. As the k_s/k_f increases, the average Nusselt decreases. As conduction mechanism through the solid material becomes of a higher importance, the relative contribution of the transport due to convective currents is reduced, leading to reduction on the numerical value Nu_w. In the limiting case, when $k_s/k_f \to \infty$, the cavity Nusselt number would tend to attain unity reflecting the fact that conduction heat transfer, in such limiting case, would be the dominant mechanism of heat transport across the cavity.

9. Effect of porosity ϕ

Porosity is another important parameter to be considered when heat transport across the cavity is investigated. For a cavity as in Fig. 1a, Nu_w represents the ratio between the sum of convection and conduction transport mechanisms over conduction transport alone. Therefore, for a purely conductive heat transfer process across the cavity, Nu_w would attain unity, as defined by Eqs. (13) and (14).

Fig. 3a indicates that as porosity decreases, Nu_w increases and differences became higher for higher values of Ra_m. All runs in Fig. 3 were performed using the High Reynolds turbulence model, the 80×80 stretched grid in Fig. 1b and $k_s/k_f=1$. The same effect also occurs for $k_s/k_f=10$ (Fig. 3b). One explanation for this behavior is that although the convective effects increase as the porosity increases, on the overall, including the conduction through the solid, the total heat transfer across the cavity is reduced, which, in turn, reduces Nu_w (see the definition of Nu_w by inspecting Eqs. (13) and (14)). Also, for the same value for Ra_m, comparing Fig. 3a and b shows that Nu_w is reduced as k_s/k_f increases, a result that is coherent with those shown in Fig. 2b where, for a larger solid-to-fluid thermal conductivity ratio, the relative importance of convective heat transport across the cavity is reduced, reducing then Nu_w.

Finally, Fig. 4 shows that indeed a higher porosity implies a lower overall wall heat flux q_w along the hot wall at $x=0$, which, in light of the definition of Nu_w by Eqs. (13) and (14), explains why the Nusselt number is reduced when ϕ increases. In spite of having more void space for the fluid to flow, the enhancement of the overall heat transport across the cavity does not occur as ϕ increases.

The reduction of Nu_w when ϕ increases can be better understood by inspecting again Fig. 4a that is plotted for $k_s/k_f=1$. In this case, the effective conductivity, which is given by $k_{eff}=\phi\, k_f+(1-\phi)k_s$ or $k_{eff}=k_f[\phi+(1-\phi)(k_s/k_f)]$, will always give k_{eff}/k_f for $k_s/k_f=1$ regardless of the value of ϕ. Therefore, the reduction on q_w as ϕ increases implies in a reduction of Nu_w by means of its definition (Eqs. (13) and (14)). A similar reasoning applies when examining Fig. 4b for $k_s/k_f=10$.

10. Conclusion

Computations for laminar and turbulent flows with the macroscopic k-ε model with wall function for natural convection in a square cavity fully filled with porous medium were performed. Results indicate that when using the one energy equation model under the turbulent regime simulated with a High Reynolds turbulence model, the cavity Nusselt number is reduced for higher values of the ratio k_s/k_f as well as when the material porosity in increased. In both cases, conduction thorough the solid material becomes of a greater importance when compared with the overall transport that includes also convective heat transport due to fluid motion. The work herein might benefit the solution of industrial problems of practical relevance.

Acknowledgments

The authors are thankful to CNPq and CAPES, Brazil, for their invaluable financial support during the course of this research.

References

[1] C.T. Hsu, P. Cheng, Thermal dispersion in a porous medium, Int. J. Heat Mass Transfer 33 (1990) 1587–1597.
[2] J. Bear, Dynamics of Fluids in Porous Media, American Elsevier Pub. Co., New York, 1972.
[3] S. Whitaker, Equations of motion in porous media, Chem. Eng. Sci. 21 (1966) 291.
[4] S. Whitaker, Diffusion and dispersion in porous media, J. Am. Inst. Chem. Eng. 13 (3) (1967) 420.
[5] T. Masuoka, Y. Takatsu, Turbulence model for flow through porous media, Int. J. Heat Mass Transfer 39 (13) (1996) 2803–2809.
[6] F. Kuwahara, A. Nakayama, H. Koyama, A numerical study of thermal dispersion in porous media, J. Heat Transf. 118 (1996) 756–761.
[7] F. Kuwahara, A. Nakayama, Numerical modeling of non-Darcy convective flow in a porous medium, Heat Transfer 1998: Proc. 11th Int. Heat Transf. Conf., Kyongyu, Korea4, Taylor & Francis, Washington, D.C., 1998, pp. 411–416.
[8] A. Nakayama, F. Kuwahara, A macroscopic turbulence model for flow in a porous medium, J. Fluids Eng. 121 (1999) 427–433.
[9] K. Lee, J.R. Howell, Forced convective and radiative transfer within a highly porous layer exposed to a turbulent external flow field, Proceedings of the 1987 ASME-JSME Thermal Engineering Joint Conf., Honolulu, Hawaii2, ASME, New York, N.Y., 1987, pp. 377–386.
[10] B.V. Antohe, J.L. Lage, A general two-equation macroscopic turbulence model for incompressible flow in porous media, Int. J. Heat Mass Transfer 40 (13) (1997) 3013–3024.
[11] D. Getachewa, W.J. Minkowycz, J.L. Lage, Int. J. Heat Mass Transfer 43 (2000) 2909.
[12] M.J.S. de Lemos, Turbulence in Porous Media: Modeling and Applications, 2nd ed. Elsevier, Amsterdam, 2012.
[13] N.C. Markatos, K.A. Pericleous, Laminar and turbulent natural convection in an enclosed cavity, Int. J. Heat Mass Transfer 27 (1984) 755–772.
[14] H. Ozoe, A. Mouri, M. Ohmuro, S.W. Churchill, N. Lior, Numerical calculations of laminar and turbulent natural convection in water in rectangular channels heated and cooled isothermally on the opposing vertical walls, Int. J. Heat Mass Transfer 28 (1985) 125–138.
[15] R.A.W.M. Henkes, F.F. Van Der Vlugt, C.J. Hoogendoorn, Natural-convection flow in a square cavity calculated with low-Reynolds-number turbulence models, Int. J. Heat Mass transfer 34 (2) (1991) 377–388.
[16] T. Fusegi, J.M. Hyun, K. Kuwahara, Three-dimensional simulations of natural convection in a sidewall-heated cube, Int. J. Numer. Methods Fluids 3 (1991) 857–867.
[17] G. Barakos, E. Mitsoulis, D. Assimacopoulos, Natural convection flow in a square cavity revited: laminar and turbulent models with wall function, Int. J. Numer. Methods Fluids 18 (1994) 695–719.
[18] D.A. Nield, A. Bejan, Convection in Porous Media, Springer, New York, 1992.
[19] D.B. Ingham, I. Pop, Transport Phenomena in Porous Media, Elsevier, Amsterdam, 1998.
[20] K.L. Walker, G.M. Homsy, Convection in Porous Cavity, J. Fluid Mech. 87 (1978) 49–474.
[21] A. Bejan, On the boundary layer regime in a vertical enclosure filled with a porous medium, Lett. Heat Mass transfer 6 (1979) 93–102.
[22] V. Prasad, F.A. Kulacki, Convective heat transfer in a rectangular porous cavity-effect of aspect ratio on flow structure and heat transfer, J. Heat Transfer 106 (1984) 158–165.
[23] C. Beckermann, R. Viskanta, S. Ramadhyani, A numerical study of non-Darcian natural convection in a vertical enclosure filled with a porous medium, Numer. Heat Transfer 10 (1986) 557–570.
[24] R.J. Gross, M.R. Bear, C.E. Hickox, The Application of Flux-corrected Transport (FCT) to High Rayleigh Number Natural Convection in a Porous Medium, Proc, 8th Int. Heat transfer Conf., San Francisco, CA, 1986, 1986.
[25] D.M. Manole, J.L. Lage, Numerical benchmark results for natural convection in a porous medium cavity, HTD-Vol 216, Heat and mass Transfer in Porous Media, ASME Conference, 1992. 55–60.
[26] S.L. Moya, E. Ramos, M. Sen, Numerical study of natural convection in a tilted rectangular porous material, Int. J. Heat Mass Transfer 30 (1987) 741–756.
[27] A.C. Baytas, I. Pop, Free convection in oblique enclosures filled with a porous medium, Int. J. Heat Mass Transfer 42 (1999) 1047–1057.
[28] E.J. Braga, M.J.S. de Lemos, Turbulent natural convection in a porous square cavity computed with a macroscopic k-ε model, Int. J. Heat Mass Transf. 47 (2004) 3650–5639.
[29] M.J.S. de Lemos, C. Fischer, Thermal analysis of an impinging jet on a plate with and without a porous layer, Numer. Heat Transfer, Part A 54 (2008) 1022–1041.
[30] B.E. Launder, D.B. Spalding, The numerical computation of turbulent flows, Comput. Methods Appl. Mech. Eng. 3 (1974) 269–289.
[31] K. Abe, Y. Nagano, T. Kondoh, An improve k-ε model for prediction of turbulent flows with separation and reattachment, Trans. JSME 58 (1992) 3003–3010.
[32] S.V. Patankar, D.B. Spalding, A calculation procedure for heat, mass and momentum transfer in three dimensional parabolic flows, Int. J. Heat Mass Transfer 15 (1972) 1787.
[33] H.L. Stone, Iterative solution of implicit approximations of multi-dimensional partial differential equations, SIAM J. Numer. Anal. 5 (1968) 530–558.